
Article:
Cox, A., Herbert, S., Villain-Chastre, J.-P. et al. (2 more authors) (2019) The effect of machining and induced surface deformation on the fatigue performance of a high strength metastable β titanium alloy. International Journal of Fatigue, 124. pp. 26-33. ISSN 0142-1123

https://doi.org/10.1016/j.ijfatigue.2019.02.033

The effect of machining and induced surface deformation on the fatigue performance of a high strength metastable β titanium alloy

A. Cox, S. Herbert, J.-P. Villain-Chastre, S. Turner, M. Jackson

PII: S0142-1123(19)30053-2
DOI: https://doi.org/10.1016/j.ijfatigue.2019.02.033
Reference: JIJF 4998

To appear in: *International Journal of Fatigue*

Received Date: 15 November 2018
Revised Date: 16 February 2019
Accepted Date: 22 February 2019

Please cite this article as: Cox, A., Herbert, S., Villain-Chastre, J.-P., Turner, S., Jackson, M., The effect of machining and induced surface deformation on the fatigue performance of a high strength metastable β titanium alloy, *International Journal of Fatigue* (2019), doi: https://doi.org/10.1016/j.ijfatigue.2019.02.033

The effect of machining and induced surface deformation on the fatigue performance of a high strength metastable β titanium alloy

A. Cox[1], S. Herbert[1], J-P, Villain-Chastre[2], S. Turner[3], M. Jackson[1]

[1]*Department of Materials Science and Engineering, The University of Sheffield, Sir Robert Hadfield Building; Mappin Street, Sheffield, S1 3JD, United Kingdom.* [2] *Safran Landing Systems; Cheltenham Road East, Gloucester, Gloucestershire, GL2 9QH, United Kingdom.* [3] *High Value Manufacturing Catapult, Regus Building, Blythe Valley Business Park, Shirley, Solihull, B90 8AG, United Kingdom.*

Abstract

Metastable beta titanium alloys such as Ti-5Al-5Mo-5V-3Cr (Ti-5553) are used for large aero-structural components. During processing these alloys are subject to costly machining operations. There is an industry demand to machine at improved metal removal rates (MRR) to meet increasing aircraft orders. To understand the effects of MRR on subsurface deformation and fatigue performance, fatigue coupons were end milled under two different industrial conditions. The surface roughness, residual stress and subsurface deformation was characterised and a custom four point bend fatigue testing was designed to determine the effect of MMR on cycles to failure. The study has demonstrated that an increase in MMR of 50% resulted in a LCF reduction of 57.37%. This was a direct result of increased subsurface damage and residual stresses.

Keywords:
Crack formation, Low cycle fatigue, Titanium alloys, Milling, Subsurface damage.

1. Introduction

State of the art commercial aircraft platforms, such as the Boeing 787 Dreamliner and Airbus A350, are utilising the advantageous mechanical properties of high strength to weight ratio titanium alloys in ever increasing quan-

tities [1]. Systematic improvements in processing and operational properties have consequentially justified the adoption of the metastable β titanium alloys Ti-10V-2Fe-3Al (Ti-10-2-3) and Ti-5Al-5Mo-5V-3Cr (Ti-5553) over well-established alloys like the general purpose α/β Ti-6Al-4V (Ti-6-4), in landing gear and load-bearing fuselage applications[1, 2, 3]. In service, such critical aero-structural components are subject to complex loading conditions and can be acutely susceptible to fatigue failures. Investigations have been conducted into fatigue mechanisms for a range of widely adopted titanium alloys [4, 5, 6, 7]. These studies show how crack initiation can dominate the fatigue life of titanium alloys [8]. Crack initiation, achieved through the activation of deformation modes, is accommodated via damage accumulation during cyclic stress application [8, 4, 9, 10, 11, 12]. For duplex phase titanium alloys, fatigue crack initiation is preferentially accommodated by the hexagonal close packed (HCP) primary alpha (α_p) phase and can be observed as subsurface dislocation slip bands [4, 8]. Fatigue facets and slip bands have been identified from fatigue failures in Ti-6-4, IMI-834 and Ti-10-2-3 [4, 13, 14]. Prevalence for dislocation slip has been found parallel to the; basal plane $\{11\bar{2}0\}(0001)$, c-axis in the $(10\bar{1}0)$ direction and the $\{12\bar{1}0\}(10\bar{1}0)$ prismatic plane within multiple α_p grains [12, 14, 4, 10]. Through the application of advanced characterisation techniques like secondary electron microscopy electron backscatter diffraction (SEM-EBSD) and transmission electron microscopy (TEM), studies have shown dislocation pile up and subsequent slip at the α/β interface [11] as a result of the inherent precipitate free zone that exists [13]. The lower critically resolved shear stress (CRSS) required to activate basal slip explains the dominance in fatigue initiation and rate of crack formation that occurs at Basal planes of α_p grains [10]. Due to microstructural and mechanical heterogeneities present for duplex titanium alloys, fatigue damage is inherently localised [8, 10, 13]. These heterogeneities produce significant statistical variations in comparable studies on fatigue mechanisms [15, 16]. This substantiates the complexities and expense of the incremental performance improvements required for these components [1, 16]. For alloys with relatively low volume fractions <10% of α_p, as for the metastable β alloys; Ti-5553 or Ti-10-2-3, competing microstructurally induced mechanisms; both surface and subsurface, are found to contribute to fatigue failure [8, 17]. However, such studies typically focus primarily on probabilistic and numeric behaviour in fatigue data rather than on mechanistic and microstructural considerations. Damage accumulation has been found to be promoted locally in macrozones, in which preferentially orientations of

α_p due to non-linear strains during forging, influenced through the Burgers relationship, by the preferential orientations local to the matrix phase, influence the susceptibility to deformation [10]. This non-uniformity found in plastic deformation is not only evident in damage accumulation by fatigue loading, but other deformational processes such as machining. The intrinsic variations in the polycrystalline Ti-6Al-4V and Ti-834 alloys influences the intensity and depth of severe plastic deformation (SPD) and induced subsurface strain as a result of milling [18]. Machining induced deformation was found to be accommodated in the same crystallographic planes as that during fatigue loading, as identified by the associated Schmid factors [4]. Machining accounts for up to 60% of overall component cost and thus the advanced manufacturing sector needs to explore increased material removal rates (MRR) to meet the challenges associated with a global surge in aircraft demand especially in Asia. It has been shown that increases in cutting speeds (V_c) and feed rates (f_z) for machining of titanium alloys can play a significant role in component integrity, increasing cutting forces; subsurface residual stresses, subsurface deformation and the propensity for the activation of deformation modes [19, 20, 21, 22, 23, 24, 25, 26]. Preceding research has focused on the importance of surface condition [27, 28, 29, 30]. However, this approach is limited and does not consider the subsurface condition, nor the interaction with the surface condition as a result of engineering operations applied to aero-components. Other work has postulated that an interaction exists [31], however, there has been insufficient work that provides a holistic assessment of fatigue performance post machining. The present study is an investigation into the influence of machining on induced deformation and the subsequent fatigue performance for aero-structural materials. The work aims to address the issues discussed and exploit opportunities to advance the application of metastable β alloys in aero-structural applications [1]. Through the application of custom low cost, small scale testing, the inherent expensive and iterative nature of development will be addressed.

2. Methods

2.1. Material

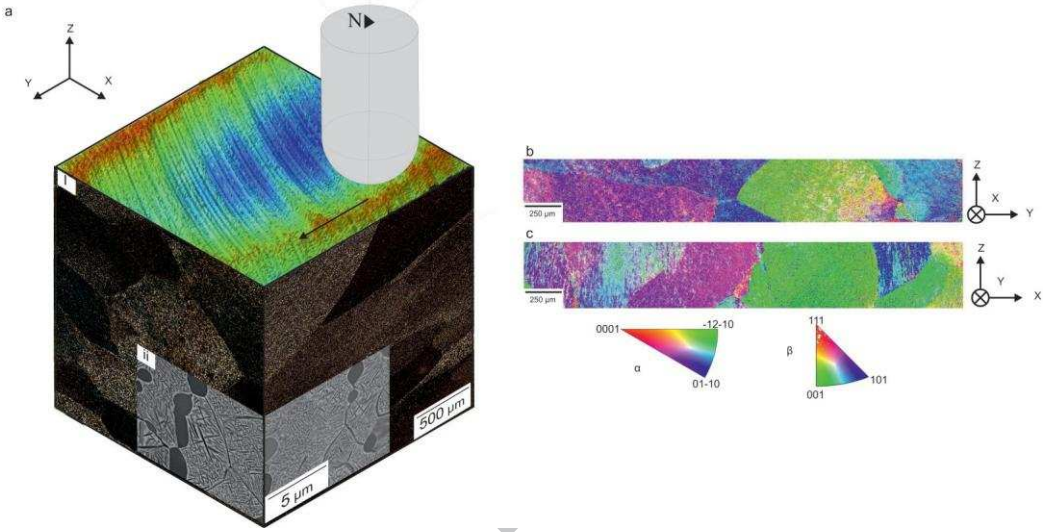

Figure 1: Schematic representation of (a.) surface and subsurface with (i.) optical micrographs and (ii.) backscatter electron images of the as-received Ti-5Al-5Mo-5V-3Cr microstructures and milled topography viewed along the radial direction (X) and axial direction (Y) with respect to milling direction. Representations of the respective pole figure contour plots and inverse pole figure (IPF) EBSD maps for the planes parallel to the (b.) X and (c.) Y planes.

The Ti-5553 alloy under investigation was supplied by VSMPO-AVISMA and Safran Landing Systems in the form of an as-recieved Boeing 787 Dreamliner truck beam section. The alloy is presented in the condition where the prior processing was a β forge followed by a subtransus solution heat treatment and age. The direction of elongation (ED), of the retained β grains as a result of the thermomechanical strain path can be observed in Fig.1a). The alloy is comprised of a bi-modal microstructure in which a volume fraction of 10±1% primary α_p is present in the form of 5 µm globular grains. The remaining body-centered cubic (BCC) β is deliniated with high aspect secondary alpha (α_s) laths, sub-micron in thickness. Large inverse pole figure (IPF) EBSD maps of the planes perpendicular to the ED and radial direction (RD) are presented along, with inverse pole figures (IPF) contour plots for

the α **{**0001**}** and β **{**110**}** planes which describes the Burgers relationship between the two phases in Fig.1b) and c). Further information regarding the influence of processing on mechanical properties for Ti-5553 can be found in the literature [2, 32, 33, 13].

2.2. Fatigue experimentation

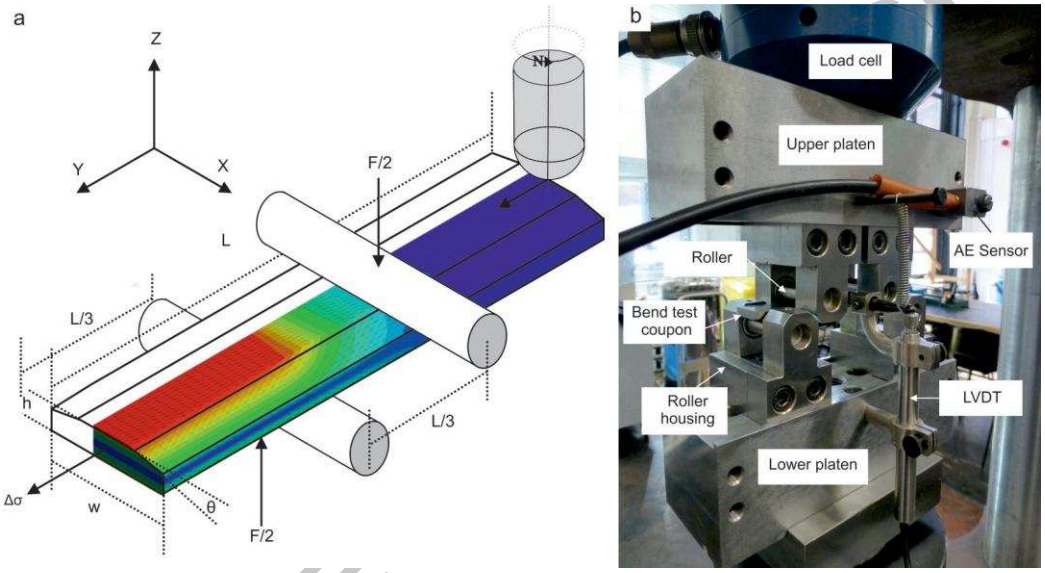

Figure 2: (a.) A cross-sectional schematic representation of the four point bend fatigue test assembly, coupon geometry and superimposed FEA stress distribution with respect to milling and microstructural directions and (b.) an annotated photograph of the four point bend fatigue test rig assembly at the University of Sheffield.

Fatigue tests were conducted at room temperature in air using a Nene 12 kN servo-hydraulic testing machine operated via a Moog SmarTEST One controller. All tests were conducted to failure within the low cycle fatigue (LCF) range under controlled load at high elastic stresses to induce local plasticity under a sinusoidal application at a frequency of 5 Hz. A stress ratio of R=0.1 with the σ_{max} = 1050 MPa was maintained throughout the fatigue test. A custom four point bend fatigue test design was applied for this study, as shown in Fig.2b, in which the load was distributed through two upper static and two lower dynamic rollers each secured within needle roller bearings set in high strength steel housings and bases. This test allowed for a large region of maximum applied tensile stress on the upper face as illustrated

Table 1: SUMMARY OF CUTTING CONDITIONS

Cutting parameter	Condition 1	Condition 2
Cutting speed (V_c) m/min	300	375
Feed per tooth (f_z) mm/tooth	0.14	0.22
Radial depth of cut (a_p) mm	0.3	0.3
Axial depth of cut (a_e) mm	0.7	0.7

by the stress contour map exported for Ansys FE analysis (Fig. 2a). Fatigue coupons were extracted from the source material via wire-EDM along the Y direction with respect to Fig.1a. The low cycle fatigue regimen employed in this study is comparable with regards to stress application and stress ratio to that found in industrial applications. Due to the none conventional nature of this testing design it was important to maintain comparable parameters throughout the study. Due to the none conventional nature of this fatigue testing design, the loading regime employed is based upon those used in industry for material and component characterisation. Due to the costly nature of the coupon fabrication and fatigue testing, a small number of machining conditions were investigated. Those chosen were based on the achievable processing window within industrial machining centres. Machining was performed on a Starrag STC 1250 5 axis machining centre producing coupons to the required geometry of 3.6, 19 and 120 mm in height (h), width (w) and length (2L) respectively Fig.2a . The chamfer angle (θ) of 100 produces an upper face of 10 mm in width. This upper face, milled with machining conditions used by Safran Landing Systems using Kennametal solid carbide 6 flute ball nose end milling tools. A high lead angle (Ψ_r) was used in order to engage the maximum effective cutting diameter (Φ_{eff}) and thus optimum MRR and tool life. Hocut 795B coolant was delivered via flood and through tool holder supply at 100 bar and 70 l/min throughout milling. In order to study the effect of increased MRR, two machining conditions were used at cutting speeds (V_c) and feed per tooth (f_z), as described in Table 1. Prior to the fatigue testing a substantial array of machining conditions were investigated with regards to the impact on machinability and tool wear [34]. A limited number of parameters were used in this study and represent those offering a substantial step change with regards to material removal rate from those typically employed in industry for this application. To replicate finish machining practises constant radial and axial depths of cut were maintained.

A third condition was produced via grinding progressively with silicon carbide grinding papers of p800 and p1200 grit and polishing with 9 μm diamond suspension and 0.06 μm colloidal silica using a Buehler Automet. This third condition was used as a benchmarking exercise to compare fatigue performance in a four point bend test design with that of conventional uniaxial testing. This latter condition was included in order to better understand the influence of machining on deformation and subsequent fatigue performance.

2.3. Characterisation techniques

Prior to fatigue testing the surface and subsurface condition for each coupon was characterised. The 3D surface topography was measured using a Bruker Contour GT optical microscope with 2D surface roughness profiles produced via a mechanical stylus utilising a Mitutoyo SurfTest SV-600 profilometer in accordance with the international standard; BS EN ISO 4288:1998. Determination of conventional roughness parameters were employed during this study to ensure compatibility with industrial testing programmes. Significant research has also been conducted throughout academia linking surface roughness with fatigue behaviour and it was determined this is a suitable benchmark to use throughout this research. The subsurface deformation, as a result of milling and polishing operations were characterised under high resolution scanning electron micrscopy (SEM) using secondary electron (SE) and back scattered electron (BSE) on FEI InspectF and InspectF50 field emission gun scanning electron microscopes (FEG SEM). The residual stress profile of all three conditions was obtained using X-ray diffraction (XRD) with a Cu source and Ni filter at 40 kV and 20 mA at Laboratoire de Mécaniqueet Technologie (LMT) Cachan, Paris. A Struers LectoPol-5 electropolishing device was used to exposure subsurface material at 35 A and 0.43 V. This provided profiles of the subsurface stress down to a depth of 200 μm obtained in both the ED and RD directions. The fracture surfaces of fatigue specimens were studied under SEM in order to characterise the mechanistic fatigue behaviour and key microstructure features that lead to failure. The nature of the four point bend fatigue test design is advantageous with regards maximum stress distribution. Samples were sectioned using a Struers Secotom-50 precision saw and imaged using high resolution BSEI. The same sectioned samples were then analysed using high magnification electron backscatter diffraction (EBSD) on a FEI Inspect F50 FEG SEM using a 0.06 μm step size at x5000 magnification.

3. Results and discussion

3.1. Machining induced surface integrity and subsurface deformation

Due to the large β grain size and strong texture possessed by the Ti-5553 alloy, there is a potential for microstructurally induced variation in mechanical properties. Fatigue behaviour between the two machining conditions and different coupons may not be accurately assessed if the material has such a variation. The source material was inspected via Vickers hardness indentation. The results of which were averaged and standard deviations calculated in the cross-sectional planes; circumferential (X) and longitudinal (Y) being 374 and 4 H_V and 373 and 5 H_V , respectively. Consistency in mechanical properties throughout the source material can be inferred and it was concluded that coupon extraction could occur from any location of the source material. The 2D and 3D surface roughness was characterised, with examples of large area stitched 3D light micrographs presented in Fig.3a and b. 2D roughness profiles were recorded across all coupons in three locations and two directions, X and Y, as shown in Fig.3a and b. Values for Ra, Rq, Sk and Ku for condition 1, were found to be; 1.353 µm, 1.576 µm, 0.244 and 2.081 (3dp), respectively. The corresponding values for condition 2, were recorded as, 1.233 µm, 1.432 µm, 0.19 and 2.135 (3dp), respectively. Values in 3D for condition 1 for the metrics Sa, SRq, SSk and SKu were 2.648 µm, 3.328 µm, 0.417 and 2.782 (3dp), respectively. The corresponding values for condition 2 were 2.961 µm, 3.708 µm, 0.455 and 2.084 (3dp), respectively.

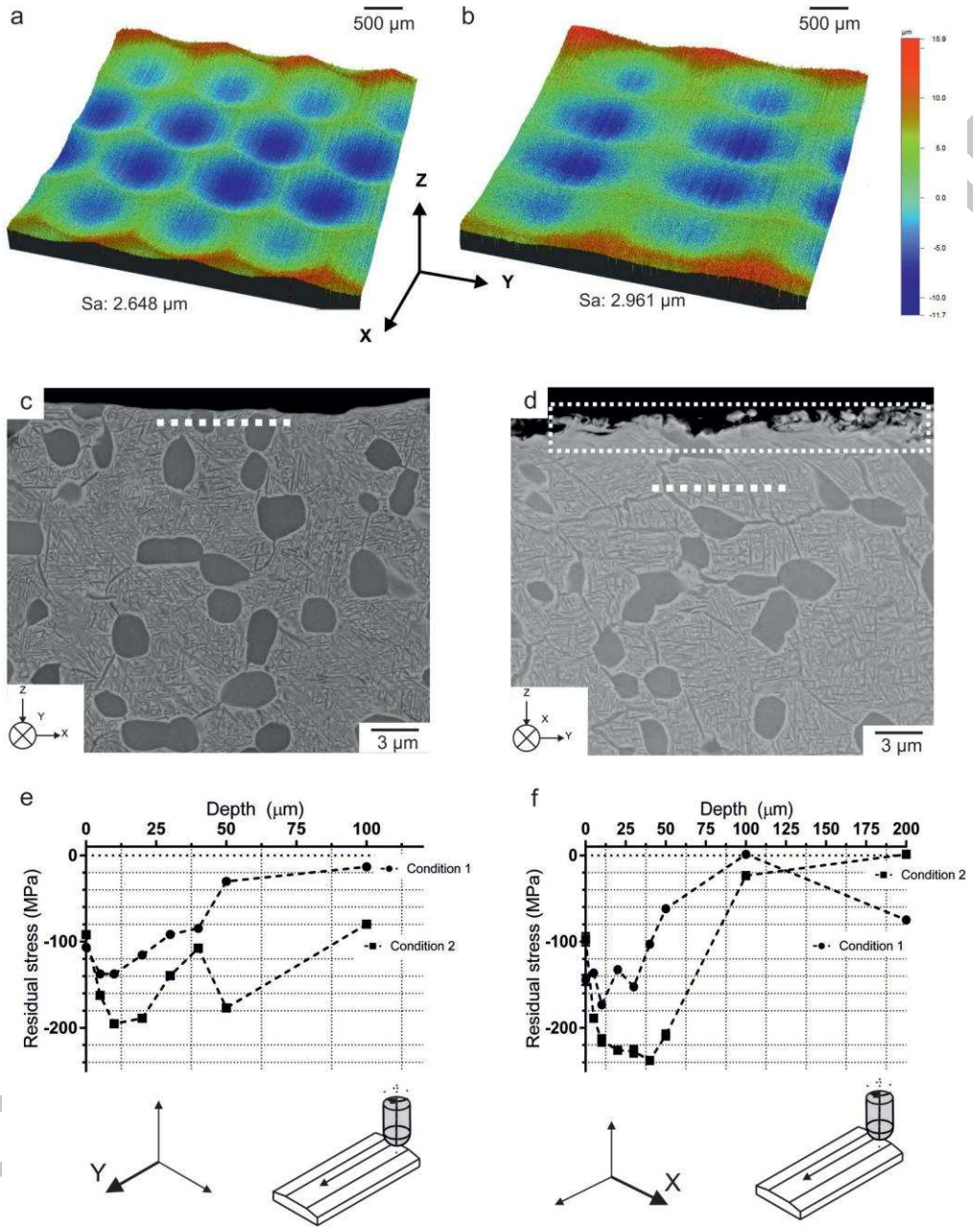

Figure 3: 3D light image at x2.5 magnification for conditions (a.) condition 1 and (b.) condition 2, BSEI at x10,000 of the finish end milled subsurface for (c.) condition 2 and (d.) condition 2 and schematic representation of the subsurface XRD residual stress profiles for conditions 1 and 2 in directions (e.) X and (f.) Y.

The as-machined subsurface microstructure, for both conditions, was characterised through BSEI, in both the X and Y orientations, as presented in Fig.3c and d. Condition 1 presents localised SPD in the upper 3 μm, seen as microstructural distortion and sweeping of the α_p grains with respect to the tool rotation direction. Limited intense dislocation slip is evident for this condition, with some low intensity, faint slip lines present in the upper 2 μm of α_p grains in the Y orientation, as shown in Fig.3. Unlike condition 1, condition 2 does show the presence of surface defects such as cavitation and tearing, as shown in Fig.3d. Deformation is exacerbated in the Y orientation, where the influence of increased f_z and cutting forces produce SPD and dislocation slip along prismatic and basal planes. The as-machined subsurface stress state for conditions 1 and 2 were characterised through XRD stress analysis and the results for both conditions are presented in the X orientation, Fig.3e and the Y orientation in Fig.3f. Measurements of the bulk material at a depth of 200 to 500 μm, for machined and polished Ti-5553 samples, showed an average residual stress of -8.099 MPa (3dp) with a standard deviation of 11.181 and a range of 36.441 MPa (3dp). It was concluded from light microscopy, that machining operations induced no residual stress below this depth. In both directions, it was found that residual stress was reduced to that of the bulk measurements at a subsurface depth of 200 μm. Results to depths of 100 μm are presented in Fig.3. In both the X and Y orientations at each depth the residual stress was found to be compressive in nature and of greater magnitude for the more aggressive condition 2. Greater compressive residual stresses were found to be evident in the X direction. In both directions, the upper 5 μm SPD region, presented compressive stresses of 106-144 MPa for condition 1 and 91-97 MPa for condition 2. In the Y orientation, the stress for both conditions peak at a depth of 10 μm with conditions 1 and 2 being 137.426 and 173.170 MPa (3dp), respectively. From this depth, residual stresses trend towards that found in the bulk, this behaviour occurs more rapidly for condition 1. Such behaviour was observed to a greater extent in the X orientation. For condition 1, in the X orientation, compressive residual stress reaches a maximum of 173 at 10 μm and 237 MPa for condition 2 at a depth for 40 μm. This result shows that compressive stresses are increased in both magnitude and depth with increased MRR. When studying the error for each measurement, which is calculated from the standard deviation (SD), it can be seen that the error decreases with depth. Surface measurements in both directions possess errors between 5.96 and 7.342 MPa (3dp), for conditions 1 and 2, respectively. This is re-

duced to 3.081 and 4.684 MPa (3dp) at a subsurface depth of 100 μm in depth. This demonstrates that the accuracy of residual stress measurements is reduced nearer the machined surface. This is due to the increased crystallographic distortion as a result of severe plastic deformation through fatigue loading. As distortion is increased, diffraction of the incident X-ray is exacerbated and quality of the measurements are reduced. It is believed with some confidence that the remainder of the bulk material has negligible stress associated with it. It is also noteworthy that no significant tensile residual stresses were recorded throughout the subsurface. Due to the increased error of near surface measurements and the size relationship between penetration depth and grain size, it is hypothesised that there is a localised tensile stress present within the upper 5 μm of the subsurface. Such tensile residuals at the surface would balance the compressive stresses present in the upper 200 μm and would explain to the increased tendency for dislocation slip within α_p grains as a result of tensile loading.

Coupons subjected to machining conditions were successfully tested to low cycle fatigue failure at applied loads of 4260 and 426 N achieving standard deviations of 5.183 and 4.945 N (3dp), respectively and thus confirming that throughout the fatigue test, a stable and accurate R = 0.1 was maintained. Through analysis of data accumulated from LVDT and the MoogTest controller, coupons subjected to condition 1 was found to be typically displaced by 2.713 mm (3dp), between the applied loads, with condition 2 exhibiting an average displacement of 2.81 mm (3dp). During the steady state phase of fatigue testing, both conditions showed negligible difference in displacement or variation in magnitude over all tests.

During the steady state portion of fatigue tests, condition 1 presented an average micro-strain of 9.895 $x10^{-3}$ and 2.64 $x10^{-3}$(3dp), for the 0 and 90 directions, respectively. The comparable measurements of microstrain for condition 2 were 9.191 $x10^{-3}$ and 3.194 $x10^{-3}$, respectively. Negligible variation in strain and therefore inferred stress is observed across both conditions in all tests.

The results of the four point bend testing for both conditions are presented in 2. Over the entire testing programme, the average normalised cycles to failure for conditions 1 and 2 were 100% and 42.63%, respectively. The upper and lower fatigue life recorded for condition 1 was 153.83% and 66.14% with the equivalent for condition 2 being 48.75% and 41.27% cycles to failure, respectively. It can be seen from these results that fatigue life has been reduced significantly with increased MRR. Excluding the anoma-

Table 2: SUMMARY OF FOUR POINT BEND FATIGUE TEST RESULTS

Cycles to failure (%)	Condition 1	Condition 2
Normalised average	100	42.63
Upper	153.83	48.75
Lower	66.4	41.27
Standard deviation	13.84	40.77

lous high cycles to failure for condition 1 at 153.83%, results showed good consistency with a standard deviation measured at 13.84% and 40.77%cycles (3dp) for conditions 1 and 2, respectively.

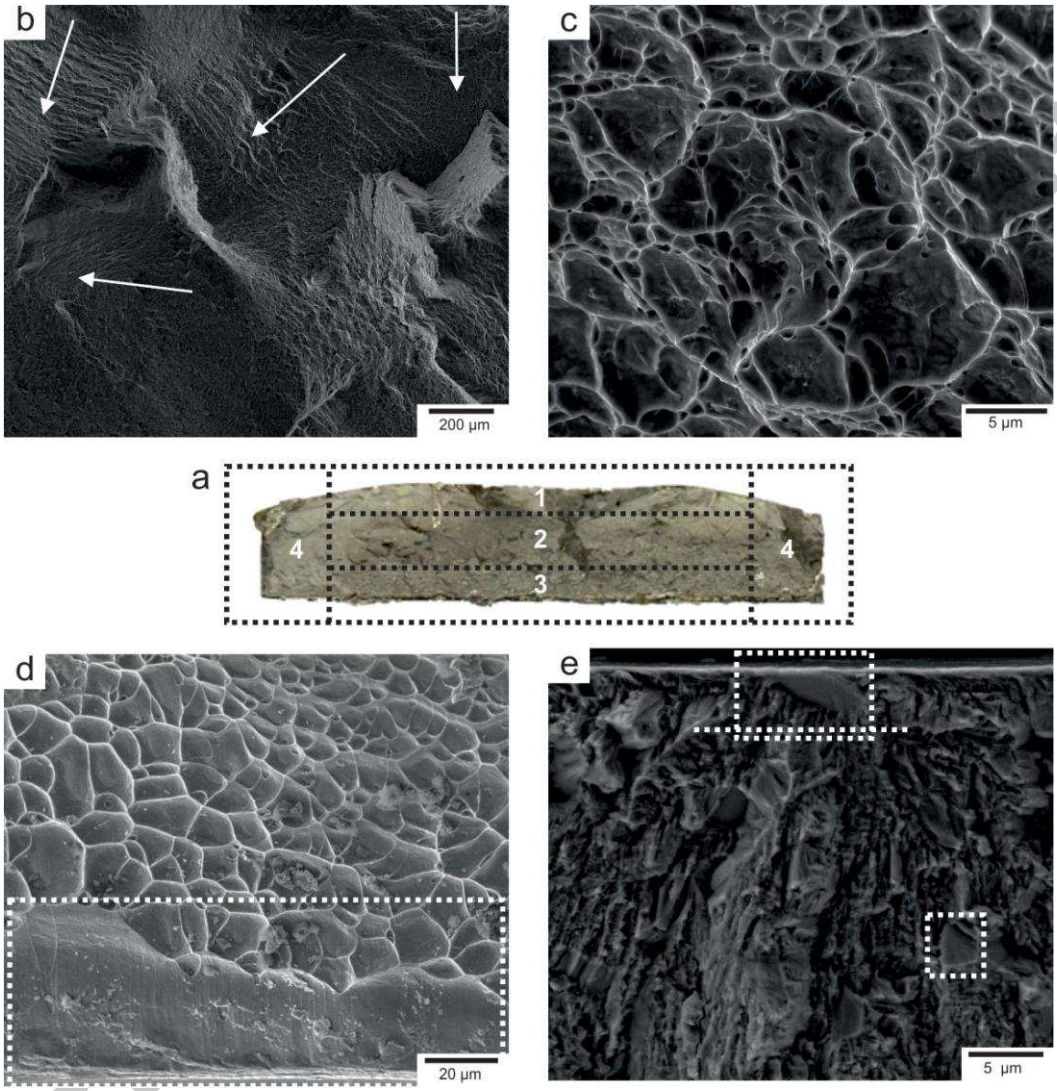

Figure 4: (a.) A typical Ti-5553 four point bend fatigue test fracture face with the four key zones highlighted; 1. upper edge of condition 1, 2. bulk of condition 1, 3. bottom edge condition 1 and 4. chamfers of condition 2 with BSEI at different magnifications presenting typical microscructural features for regions (b.) fatigue crack initiation (c.) chamfer (d.) bulk and (e.) bottom edge.

All failures occurred within the maximum surface stress region of the coupons, represented by the red region of contour schematic in Fig.1. A typical fracture face is presented in Fig.4a. The fracture face can be subdivided into four fundamental zones, to describe the failure behaviour. Region 4, is

defined as the chamfer region. On the microscopic scale, as shown in Fig.4a, this region is characterised by large serrated features, with evidence of gross plastic deformation and necking.

The bulk region 2 is defined by a many faceted surface with a range of orientations present. The bulk material presented in region 2 shows evidence of gross ductile failure, as is expected with a metastable β titanium alloy, but also localised brittle fracture. The white arrows superimposed on Fig.4b, depict the orientations of crack growth. Individual β grain orientations influence the direction of crack propagation. These directional regions of fracture are on a comparable scale of that of the β grains, like those shown in Fig.1a. The large faceted regions, delineated with dashed white boxes in Fig.4b, are evidence of gross brittle fracture which is intergranular in nature along brittle α at β grain boundaries, like that observed in Fig.1b. These regions show localised preferential orientations as a result of crystallographic texture of the large grained β phase. Under high magnification BSEI the bulk fracture texture can be clearly seen in Fig.4c. Striations and secondary cracks propagating in the direction away from origin are present on a scale comparable to the subgrain β structure. These present a mixed mode of ductile shallow dimples on brittle facets, at a scale comparable to the α_p grains, Fig.4.

Region 3, defined as the bottom edge, shows evidence of a flat face, with a burnished appearance. When studying region 3 under BSEI,Fig.4d, a distinct transition in the fracture surface can be observed. At the bottom edge of the fracture face, a pronounced fast fracture zone is delineated by the dashed white box, see Fig.4d. Fast fracture zones across both conditions were typically found to range from 200 to 600 μm in depth, irrespective of fatigue life. Within this fast fracture zone, localised regions of mixed mode failure are observed, Fig.4d with ductile equixed dimples and smooth brittle fracture faces. Under high magnification BSEI, the majority of the fast facture zone consists of elongated dimples in the direction of final failure. The severe elongation and shallow depth of these dimples, Fig.4c and d represent a low number of cycles, typical of material subject to final fast fracture.

Region 1 is characterised by the presence of crack initiation sites influenced by machining subsurface deformation. As shown in Fig.4b and c, evidence of micro void formation is present and based on the scale at which this occurs, it is believed this propagates along α⁄β grain interfaces. It was determined that no cracks initiated failure within this region. This is supported by the FEA investigation in which the material within the chamfers are subject to the lowest surface tensile stresses. From a fractography inves-

tigation, it is believed that final failure propagates through these regions in a ductile manner, with regions of shear lip formation and localised necking.

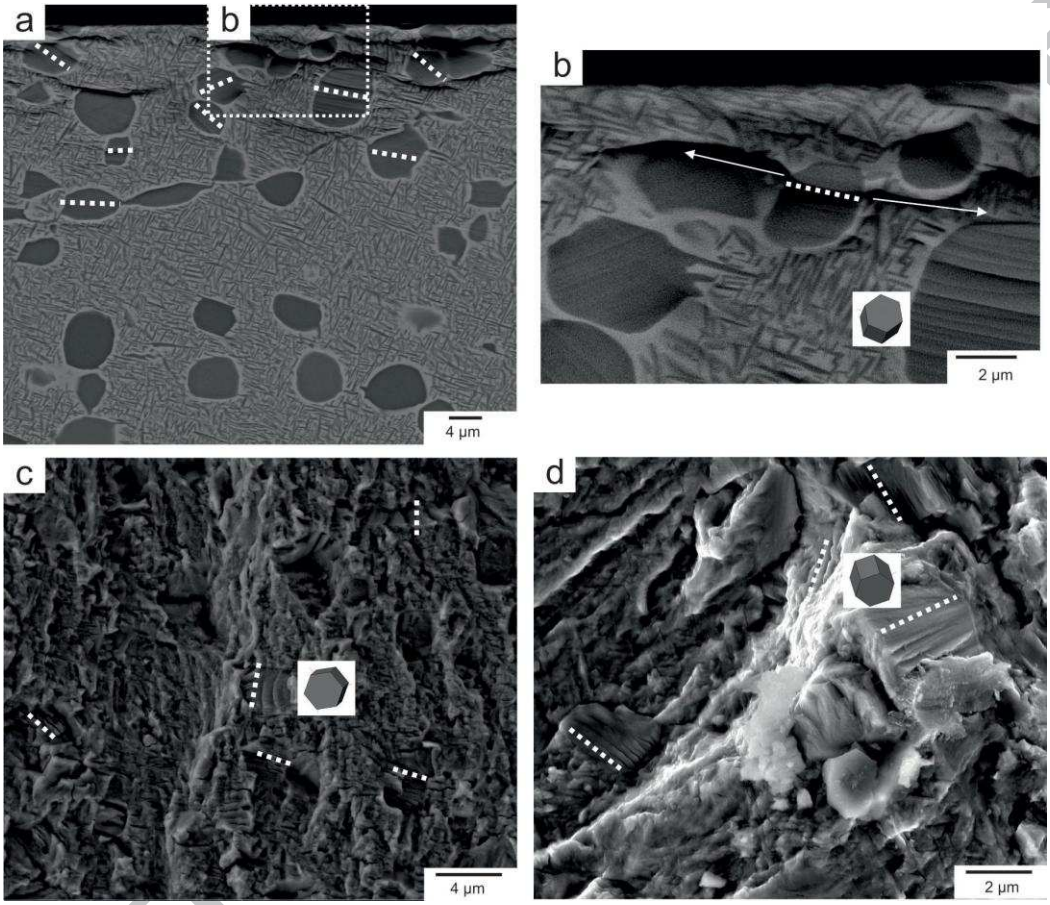

Figure 5: BSEI of condition 2, α_p grains within the (a & b.) initiation and (c and d) growth regions of the four point bend fatigue test fracture face with dominant slip directions identified by dashed line, the depth of severe plastic deformation with solid lines and crystallographic orientations of HCP α_p grains possessing dislocation slip.

For both conditions across all tests conducted, fatigue cracks were observed to initiate at the upper machined edge of the coupons within regions of severe plastic deformation. This is the surface subjected to the ball nose finish end milling operation and the region subjected to the greatest imparted deformation. Initiation zones were identifiable during inspection, as large semi-circular regions up to 250 µm in diameter. These regions possess macroscopic and microscopic striations propagating from a specific surface

location. These striations, depicted in Fig.5 b,c and d by the white arrows, suggest strain localisation within the region, which is further delineated by the dashed white box in Fig.5a, which is magnified in Fig.5b. Within this upper 50 μm initiation region, a defined mixed mode fracture surface of fibrous and dimpled ductile fracture within the β matrix face and faceted α grains are present as shown in Fig.5c. In many cases, initiation is localised and can be distinguished by a single deformed α_p grain. grains directly located at the machined surface present quasi-cleavage facet fracture features. Such fatigue behaviour in duplex titanium alloys have been reported in literature [35, 10, 4]. Evidence of numerous failure modes can be observed within this initiation region, including cleavage and fatigue striations within α grains. When compared to subsurface analysis prior to fatigue testing, with BSEI on identical scales, the influence of machining can be interpreted from fractography as is shown in Fig.5. Microstructures of α_p can be easily distinguished along with the subsurface SPD and swept grain structures local to the machined surface. It is inferred from previous results in this paper and in the literature [35, 10, 4] that this has occurred due to a combination of factors. Under high magnification BSEI within the upper 50 μm of the initiation zones presented in Fig.5, α_p grains present facets with an array of differently orientated slip lines, fatigue striations and micro cracks. Examples of such grains from both conditions are shown in Fig.5, with slip lines and microcracks highlighted with dashed white lines. Outside of this localised region, transgranular brittle cleavage and slip plane activation could not be identified. Some α_p grains did however present evidence of fatigue striations. An observable behaviour that differentiated the two cutting conditions was an increased prevalence of microcracking induced through the more aggressive machining parameters in condition 2 Fig.5 a and e. This is believed to be as a result of increased pre-existing activation of dislocation slip planes, SPD and increased localised residual stress as a result of machining prior to fatigue testing. Similar progressive damage accumulation through activation of slip planes resulting in strain localisation and eventual trans-granular fracture has been shown for Ti-5553 and other duplex titanium alloys during fatigue loading [36, 37, 35, 4]. In order to characterise the material condition prior to fatigue testing the subsurface microstructure was studied through BSEI of samples removed from just behind the fracture point as shown in Fig.4. Examples of this analysis for conditions 1 and 2 are presented in Fig.5b,c and d. Comparable depths of dislocation slip are present for both conditions. There is also evidence of localisation of those α grains exhibiting slip planes relating

to the preferential orientations of parent β grains. Slip lines are more readily observed in material subject to the more aggressive machining parameters in condition 2. The most significant instance of subsurface deformation as a result of machining and subsequent fatigue testing was found in material behind the fatigue fracture and is presented in Fig.5. High resolution BSEI, shows substantial and intense slip band formation in α_p grains in the upper 10 μm of the machining subsurface, Fig.5a and b. Fig.5, shows the progression, from machining induced deformation, through to the activation of dislocation slip, strain localisation and coalescence of micro-cracks in fatigue. Propagation of these micro-cracks persists along α⁄β grain boundaries, as shown in Fig.5c. This suggests localisation due to β orientation and subsequent α grain orientation, with respect to imposed stress from machining and subsequent strain localisation during fatigue testing.

The intense subsurface deformation identified in Fig.5 was subject to EBSD to determine the direction and plane orientations of the intense dislocation slip present. Due to the intensity of the SPD, the resolution of indexed points was low, however, to counter this, a high magnification and small step size was utilised. The plane and direction of slip was found in those α_p grains possessing no micro-cracking. Those α_p grains found to have initiated micro-cracking possessed dislocation slip in the $\{11\bar{2}0\}$ direction and the $\{00\bar{0}1\}$ plane, as with the grain in Fig.5c. Initiation of basal plane cracks have been identified in fatigue behaviour of other titanium alloys (Bridier2005,Bridier2008a). Detailed subsurface EBSD studies were conducted of subsurface material in the direct local proximity of the fatigue failure. Grains possessing slip bands and microcracks are identified in Fig.5, with 3D crystallographic orientations of α_p grains presenting dislocation slip lines in Fig.5b-e. This particular region of interest presented lower levels of strain which allowed for improved indexing when compared to Fig.5. Dislocation slip was found to have been activated along pyramidal $\{\bar{1}101\}$ and $\{1\bar{2}1\bar{3}\}$ planes and pristmatic $\{\bar{1}011\}$ and $\{\bar{1}010\}$ planes. It is believed under fatigue loading dislocation slip is activated along these crystallographic planes along basal planes led to subsurface microcracking which eventually propagate catastrophic fatigue failure.

4. Conclusions

This paper has demonstrated that the milling of four point fatigue specimens is an effective technique for assessing machining induced subsurface

plastic deformation of titanium alloy substrates and can be applied to a range of alloys and machining parameters.
For both machined conditions, within the machining induced severe plastic deformation region, intense dislocation slip was observed along basal $\{11\bar{2}0\}$, prismatic, $\{\bar{1}010\}$ and pyramidal $\{\bar{1}\bar{1}01\}$ planes. For the commercial high strength titanium alloy Ti-5553 used in large landing gear forgings, the study demonstrated that despite increased compressive residual stress profiles in the higher surface speeds, increasing the metal removal rate by 50% reduced the number of cycles to failure in LCF mode by 50%.
In all cases, micro-cracking along unfavourably aligned basal planes in the alpha phase at the machined subsurface was the dominant crack initiation mechanism, followed by ductile crack propagation through the bulk. As the alignment of such basal planes are a result of the upstream forging process, modifications to the thermomechanical processing prior to machining could increase the service life of such components post machining.

5. References

[1] James D. Cotton, Robert D. Briggs, Rodney R. Boyer, Sesh Tamirisakandala, Patrick Russo, Nikolay Shchetnikov, and John C. Fanning. State of the Art in Beta Titanium Alloys for Airframe Applications. Jom, 67(6):1281–1303, 2015. ISSN 1047-4838. doi: 10.1007/s11837-015-1442-4. URL http://link.springer.com/10.1007/s11837-015-1442-4.

[2] J.C. Fanning. Properties of TIMETAL 555 (Ti-5Al-5Mo-5V-3Cr-0.6Fe). Journal of Materials Engineering and Performance, 14(6):788–791, dec 2005. ISSN 10599495. doi: 10.1361/105994905X75628. URL http://link.springer.com/10.1361/105994905X75628.

[3] S.L. Nyakana, J.C. Fanning, and R.R. Boyer. Quick Reference Guide for β Titanium Alloys in the 00s. Journal of Materials Engineering and Performance, 14(6):799–811, dec 2005. ISSN 10599495. doi: 10.1361/105994905X75646. URL http://link.springer.com/10.1361/105994905X75646.

[4] G J Baxter, W M Rainforth, and L Grabowski. TEM observations of fatigue damage accumulation at the surface of near alpha Titanium alloy IMI 834. 44(9):3453–3463, 1996.

[5] J.A Hall. Fatigue crack initiation in alpha-beta titanium alloys. International Journal of Fatigue, 19(93):23–37, 1997. ISSN 01421123. doi: 10.1016/S0142-1123(97)00047-9.

[6] Gerd Lutjering and James C. Williams. Titanium. Springer, 2007.

[7] C Leyens and M Peters, editors. Titanium and Titanium Alloys. Wiley-VCH, 2003. ISBN 3527305343.

[8] Sushant K. Jha, Christopher J. Szczepanski, Reji John, and James M. Larsen. Deformation heterogeneities and their role in life-limiting fatigue failures in a two-phase titanium alloy. Acta Materialia, 82(2015):378–395, 2015. ISSN 13596454. doi: 10.1016/j.actamat.2014.08.034. URL http://dx.doi.org/10.1016/j.actamat.2014.08.034.

[9] M R Bache, W J Evans, and H M Davies. Electron back scattered diffraction (EBSD) analysis of quasi-cleavage and hydrogen induced fractures under cyclic and dwell loading in titanium alloys . Journal of Materials Science, 32(13):3435–3442, 1997. ISSN 00222461. doi: 10.1023/A:1018624801310. URL http://www.springerlink.com/openurl.asp?id=doi:10.1023/A:1018624801310.

[10] F. Bridier, P. Villechaise, and J. Mendez. Slip and fatigue crack formation processes in an α/β titanium alloy in relation to crystallographic texture on different scales. Acta Materialia, 56(15):3951–3962, sep 2008. ISSN 13596454. doi: 10.1016/j.actamat.2008.04.036. URL http://linkinghub.elsevier.com/retrieve/pii/S1359645408002917.

[11] A. L. Pilchak, R. E A Williams, and J. C. Williams. Crystallography of fatigue crack initiation and growth in fully lamellar Ti-6Al-4V. Metallurgical and Materials Transactions A: Physical Metallurgy and Materials Science, 41(1):106–124, 2010. ISSN 10735623. doi: 10.1007/s11661-009-0064-2.

[12] P. O. Tympel, T. C. Lindley, E. A. Saunders, M. Dixon, and D. Dye. Influence of complex LCF and dwell load regimes on fatigue of Ti-6Al-4V. Acta Materialia, 103(2016):77–88, 2016. ISSN 13596454. doi: 10.1016/j.actamat.2015.09.014. URL http://dx.doi.org/10.1016/j.actamat.2015.09.014.

[13] Jun Huang, Zhirui Wang, and Kemin Xue. Cyclic deformation response and micromechanisms of Ti alloy Ti5Al5V5Mo3Cr0.5Fe. Materials Science and Engineering: A, 528(29-30):8723–8732, nov 2011. ISSN 09215093. doi: 10.1016/j.msea.2011.08.045. URL http://linkinghub.elsevier.com/retrieve/pii/S0921509311009397.

[14] Sushant K. Jha, Christopher J. Szczepanski, Patrick J. Golden, William J. Porter, and Reji John. Characterization of fatigue crack-initiation facets in relation to lifetime variability in Ti-6Al-4V. International Journal of Fatigue, 42:248–257, 2012. ISSN 01421123. doi: 10.1016/j.ijfatigue.2011.11.017.

[15] S. K. Jha, J. M. Larsen, and A. H. Rosenberger. Towards a physics-based description of fatigue variability behavior in probabilis- tic life-prediction. Engineering Fracture Mechanics, 76(5):681–694, 2009. ISSN 00137944. doi: 10.1016/j.engfracmech.2008.10.013. URL http://dx.doi.org/10.1016/j.engfracmech.2008.10.013.

[16] K. S. Ravi Chandran, P. Chang, and G. T. Cashman. Competing failure modes and complex S-N curves in fatigue of structural materials. International Journal of Fatigue, 32(3):482–491, 2010. ISSN 01421123. doi: 10.1016/j.ijfatigue.2009.08.004.

[17] S. K. Jha and K. S Ravi Chandran. An unusual fatigue phenomenon: Duality of the S-N fatigue curve in the Beta titanium alloy Ti-10V-2Fe-3Al. Scripta Materialia, 48(8):1207–1212, 2003. ISSN 13596462. doi: 10.1016/S1359-6462(02)00565-1.

[18] Meurig Thomas, Sam Turner,and Martin Jackson. Microstructural damage during high-speed milling of titanium alloys. Scripta Materialia, 62(5):250–253, mar 2010. ISSN 13596462. doi: 10.1016/j.scriptamat.2009.11.009. URL http://linkinghub.elsevier.com/retrieve/pii/S1359646209007118.

[19] C.H Che-Haron. Tool life and surface integrity in turning titanium alloy, volume 118. dec 2001. doi: 10.1016/S0924-0136(01)00926-8. URL http://linkinghub.elsevier.com/retrieve/pii/S0924013601009268.

[20] C.H. Che-Haron and a. Jawaid. The effect of machining on surface integrity of titanium alloy Ti6 Journal of Materials Processing Technology, 166(2):188–192, aug 2005. ISSN

09240136. doi: 10.1016/j.jmatprotec.2004.08.012. URL http://linkinghub.elsevier.com/retrieve/pii/S0924013604010313.

[21] J. Sun and Y.B. Guo. A comprehensive experimental study on surface integrity by end milling Ti6Al4V. Journal of Materials Processing Technology, 209(8):4036–4042, apr 2009. ISSN 09240136. doi: 10.1016/j.jmatprotec.2008.09.022. URL http://linkinghub.elsevier.com/retrieve/pii/S0924013608007061.

[22] Pete Crawforth. Towards a Micromechanistic Understanding of Imparted Subsurface Deformation During Machining of Titanium Alloys. (September):281, 2014. URL http://etheses.whiterose.ac.uk/7155/1/Pete Crawforth Thesis-Double sided printing.pdf.

[23] Pete Crawforth, Bradley Wynne, Sam Turner, and Martin Jackson. Subsurface deformation during precision turning of a near-alpha titanium alloy. Scripta Materialia, 67(10):842–845, nov 2012. ISSN 13596462. doi: 10.1016/j.scriptamat.2012.08.001. URL http://linkinghub.elsevier.com/retrieve/pii/S1359646212005118.

[24] Pete Crawforth, Chris M. Taylor, and Sam Turner. The Influence of Alloy Chemistry on the Cutting Performance and Deformation Kinetics of Titanium Alloys during Turning. Procedia CIRP, 45:151–154, 2016. ISSN 22128271. doi: 10.1016/j.procir.2016.02.167. URL http://dx.doi.org/10.1016/j.procir.2016.02.167.

[25] Matthew Simon Dargusch, Ming Xing Zhang, Suresh Palanisamy, Alexander John Michael Buddery, and David Henry StJohn. Subsurface deformation after dry machining of grade 2 titanium. Advanced Engineering Materials, 10(1-2):85–88, 2008. ISSN 14381656. doi: 10.1002/adem.200700233.

[26] Rachid M'Saoubi, Tommy Larsson, José Outeiro, Yang Guo, Sergey Suslov, Christopher Saldana, and Srinivasan Chandrasekar. Surface integrity analysis of machined Inconel 718 over multiple length scales. CIRP Annals - Manufacturing Technology, 61(1):99–102, jan 2012. ISSN 00078506. doi: 10.1016/j.cirp.2012.03.058. URL http://linkinghub.elsevier.com/retrieve/pii/S0007850612000601.

[27] M Suraratchai, J Limido, C Mabru, and R Chieragatti. Modelling the influence of machined surface roughness on the fatigue life of aluminium alloy. International Journal of Fatigue, 30(12):2119–2126, dec 2008. ISSN 01421123. doi: 10.1016/j.ijfatigue.2008.06.003. URL http://linkinghub.elsevier.com/retrieve/pii/S0142112308001692.

[28] R.C. Dewes, D.K. Aspinwall, W. Voice, P. Bowen, and D. Novovic. The effect of machined topography and integrity on fatigue life. International Journal of Machine Tools and Manufacture, 44(2-3):125–134, 2004. ISSN 08906955. doi: 10.1016/j.ijmachtools.2003.10.018.

[29] a. Souto-Lebel, N. Guillemot, C. Lartigue, and R. Billardon. Characterization and influence of defect size distribution induced by ball-end finishing milling on fatigue life. Procedia Engineering, 19:343–348, jan 2011. ISSN 18777058. doi: 10.1016/j.proeng.2011.11.123. URL http://linkinghub.elsevier.com/retrieve/pii/S1877705811029328.

[30] N. Guillemot, C. Lartigue, R. Billardon, and B. K. Mawussi. Prediction of the endurance limit taking account of the micro-geometry after finishing milling. International Journal on Interactive Design and Manufacturing (IJIDeM), 4(4):239–249, oct 2010. ISSN 1955-2513. doi: 10.1007/s12008-010-0104-6. URL http://link.springer.com/10.1007/s12008-010-0104-6.

[31] I.S. Jawahir, E. Brinksmeier, R. M'Saoubi, D.K. Aspinwall, J.C. Outeiro, D. Meyer, D. Umbrello, and a.D. Jayal. Surface integrity in material removal processes: Recent advances. CIRP Annals - Manufacturing Technology, 60(2):603–626, jan 2011. ISSN 00078506. doi: 10.1016/j.cirp.2011.05.002. URL http://linkinghub.elsevier.com/retrieve/pii/S0007850611002046.

[32] N.G. Jones, R.J. Dashwood, D. Dye, and M. Jackson. The Flow Behavior and Microstructural Evolution of Ti-5Al-5Mo- 5V-3Cr during Subtransus Isothermal Forging. Metallurgical and Materials Transactions A, 40(8):1944–1954, jun 2009. ISSN 1073-5623. doi: 10.1007/s11661-009-9866-5. URL http://www.springerlink.com/index/10.1007/s11661-009-9866-5.

[33] N.G. Jones, R.J. Dashwood, D. Dye, and M. Jackson. Thermomechanical processing of Ti5Al5Mo5V3Cr. Mate-

rials Science and Engineering A, A 490:9, 2008. URL http://www.sciencedirect.com/science/article/pii/S0921509308001007.

[34] Adam Cox. Understanding the effect of surface generation rates for finish milling of Ti-5Al-5Mo-5V-3Cr aerostructural components. PhD thesis, University of Sheffield, 2017. URL http://etheses.whiterose.ac.uk/id/eprint/18908.

[35] F. Bridier, P. Villechaise, and J. Mendez. Analysis of the different slip systems activated by tension in a alpha-beta titanium alloy in relation with local crystallographic orientation. Acta Materialia, 53(3):555–567, 2005. ISSN 13596454. doi: 10.1016/j.actamat.2004.09.040.

[36] Dongyang Qin, Yulong Li, Shuangyin Zhang, and Lian Zhou. On the tensile embrittlement of lamellar Ti-5Al-5V-5Mo-3Cr alloy. Journal of Alloys and Compounds, 663:581–593, 2016. ISSN 09258388. doi: 10.1016/j.jallcom.2015.12.158. URL http://dx.doi.org/10.1016/j.jallcom.2015.12.158.

[37] K. Zhang, K.V. Yang, A. Huang, X. Wu, and C.H.J. Davies. Fatigue crack initiation in as forged Ti6Al4V bars with macrozones present. International Journal of Fatigue, 80(2015):288–297, 2015. ISSN 01421123. doi: 10.1016/j.ijfatigue.2015.05.020. URL http://www.sciencedirect.com/science/article/pii/S0142112315001772.

Highlights

1. Four point fatigue testing is effectively determines machining subsurface deformation
2. Bespoke machining and fatigue testing technique is applicable to a range of aerospace materials
3. Increased metal removal rates of 50% reduced of cycles to failure in low cycle failure mode by 50%
4. Dominant crack initiation in Ti-5553 is alpha basal planes at the machined subsurface
5. Modifications to the upstream forging prior to machining could increase Ti-5553 service life